Available online at www.sciencedirect.com
SCIENCE DIRECT®
International Journal of Thermal Sciences 42 (2003) 1129–1143
International Journal of Thermal Sciences
www.elsevier.com/locate/ijts

Local convective heat exchanges and flow structure in a rotor–stator system

Echanges de chaleur convectifs locaux et structure d'écoulement sur un système rotor–stator

Rachid Boutarfa *, Souad Harmand

Laboratoire de mécanique et energétique, Université de Valenciennes et du Hainaut Cambrésis, Le Mont Houy, 59313 Valenciennes cedex 9, France

Received 15 April 2002; accepted 5 March 2003

Abstract

This work deals with an experimental study of the flow structure and the local convective exchanges in the air-gap of a rotor–stator system. The experimental technique uses infrared thermography to measure the surface temperatures of the rotor and the numerical solution of the steady state heat equation to determine the local heat transfer coefficients. The analysis of the flow structure between the rotor and the stator is obtained by PIV (Particle Image Velocimetry). Tests are carried out for rotational Reynolds numbers ranging from 5.87×10^4 to 1.76×10^5 and for gap ratios ranging from 0.01 to 0.17. Analysis of the experimental results has determined the influence of the rotational Reynolds number and the gap ratio on the flow structure and the convective exchanges in the gap between the rotor and the stator. Some correlations expressing the local Nusselt number as a function of the rotational Reynolds number and the gap ratio are proposed.
© 2003 Éditions scientifiques et médicales Elsevier SAS. All rights reserved.

Résumé

Ce travail concerne l'étude expérimentale de la structure d'écoulement et des échanges convectifs locaux dans l'entrefer d'un système rotor/stator. La technique expérimentale employée est basée sur la thermographie infrarouge pour accéder à la mesure des températures de surface, et sur la résolution numérique de l'équation de l'énergie en régime stationnaire, pour évaluer les coefficients convectifs locaux. L'analyse de la structure de l'écoulement entre le rotor et le stator est obtenue à l'aide de la PIV (Vélocimétrie par Images de Particules). Les essais sont réalisés pour des nombres de Reynolds rotationnels compris entre $5{,}87 \times 10^4$ et $1{,}76 \times 10^5$, et pour des espacements adimensionnés entre le rotor et le stator compris entre 0,01 et 0,17. L'analyse des résultats expérimentaux a permis de mettre en évidence l'influence du nombre de Reynolds rotationnel et de l'espacement adimensionné sur la structure de l'écoulement et sur les échanges convectifs dans l'entrefer entre le rotor et le stator. Des corrélations reliant le nombre de Nusselt local au nombre de Reynolds rotationnel et à l'espacement adimensionné sont proposées.
© 2003 Éditions scientifiques et médicales Elsevier SAS. All rights reserved.

Keywords: Rotor; Stator; Rotating machinery; Heat transfer; Forced convection; Flow structure; Infrared thermography

Mots-clés : Rotor ; Stator ; Machine tournante ; Transfert de chaleur ; Convection forcée ; Structure d'écoulement ; Thermographie infrarouge

1. Introduction

This work is the continuation of the study of local convective heat exchanges from a rotating disc with and without a stator [1,2]. These earlier studies presented the experimental technique used to determine the local heat transfer coefficients on the rotating disc and highlighted the influence of the stator presence on the convective exchange from the rotating disc. The size and the optimization of the cooling systems of the rotating machines require a good knowledge of the flow structure and local convective exchanges on their surface. These two elements depend strongly on the machine's geometry and the temperature

* Corresponding author.
E-mail address: rachid.boutarfa@univ-valenciennes.fr (R. Boutarfa).

1290-0729/$ – see front matter © 2003 Éditions scientifiques et médicales Elsevier SAS. All rights reserved.
doi:10.1016/S1290-0729(03)00092-9

Nomenclature

c	constant
C_m	$= 2M/\rho\omega^2 R_2^5$ moment coefficient for one side of the rotor
C_w	$= Q_m/\mu r$, mass flow rate coefficient
G	$= s/R_2$, gap ratio
h	local heat transfer coefficient ..... $W\cdot m^{-2}\cdot K^{-1}$
J	radiosity ..... $W\cdot m^{-2}$
Q_m	mass flow rate ..... $kg\cdot s^{-1}$
M	moment on one side of the rotor .... $kg\cdot m^2\cdot s^{-2}$
n	constant
Nu	$= hr/\lambda_a$, local Nusselt number on the rotor
$\overline{Nu}$	mean Nusselt number on the rotor
Nu_∞	local Nusselt number on the free disc
$\overline{Nu}_\infty$	mean Nusselt number on the free disc
r	radial coordinate on the rotor ..... m
R_1	inner radius of the study zone ..... m
R_2	outer radius of the study zone ..... m
r^*	$= (r - R_1)/(R_2 - R_1)$ dimensionless radius
Re	$= \omega R_2^2/\nu$, peripheral rotational Reynolds number
Re^*	$= \omega r^2/\nu$, local Reynolds number
Re_s	$= \omega s^2/\nu_a$, gap Reynolds number
s	rotor/stator spacing ..... m
T	temperature ..... K
U_r	radial velocity component ..... $m\cdot s^{-1}$
U_θ	tangential velocity component ..... $m\cdot s^{-1}$
x	$= r/R_2$, dimensionless radius

Greek symbols

ε	emissivity
λ	thermal conductivity ..... $W\cdot m^{-1}\cdot K^{-1}$
μ	dynamic viscosity ..... $kg\cdot m^{-1}\cdot s^{-1}$
ν	kinematic viscosity ..... $m^2\cdot s^{-1}$
σ	Stefan–Boltzmann's constant .... $W\cdot m^{-2}\cdot K^{-4}$
φ	heat flux ..... $W\cdot m^{-2}$
ω	rotational speed ..... $rad\cdot s^{-1}$

Subscripts

a	air
cd	conductive
cv	convective
lim	limit
ray	radiation
r	rotor
s	stator
∞	value far from the boundary layer

distribution laws of their surface exposed to air-cooling. The objective of this work is to study the cooling of a wind turbine discoïdal alternator whose rotating part (rotor), is facing a fixed disk (stator).

The local convective exchanges between the air and the rotor surface, facing an annular stator at a distance s from the rotor (Fig. 1(a) and (b)), are determined on the rotor surface between the radii R_1 and R_2.

In this work, an experimental set-up was used to determine the local heat transfer coefficients. This experimental set-up (Fig. 1(a) and (b)) is composed of a rotating and fixed disc and uses infrared thermography to determine the surface temperatures of the rotor. The evaluation of the local heat transfer coefficient with the air is carried out on the rotor in thermal steady state. The rotor is facing a stator of inner radius $R_1 = 170$ mm and outer radius $R_2 = 290$ mm, and the gap between the two discs, s, varies from 3 to 50 mm in all the tests. The experimental set-up was adapted to carry out measurements, by PIV, of the mean field air velocities in different planes ((a), (b) and (c)) between the rotor and the stator. The tests are carried out for rotational speeds ranging between 100 and 300 rev·min^{-1} ($5.87 \times 10^4 \leqslant Re \leqslant 1.76 \times 10^5$), and for different gap ratios ($0.01 \leqslant G \leqslant 0.17$).

Studies of the flow tructure and the convective heat transfer in rotor–stator systems are largely documented, but generally concern shrouded geometrical configuration. The local convective heat transfers in the unshrouded rotor–stator systems are less documented. Only the mean convective heat transfers on a few number of unshrouded systems have been studied. The work presented in this paper is however linked to the determination of the local convective exchanges in an unshrouded rotor–stator system. This work highlights the influence of the dimensionless parameters (Re and G) on the flow structure and the convective exchanges and puts forward some correlations linking the local Nusselt number to Re and G.

2. Literature review

The convective heat transfer from a rotating disc has been the subject of numerous studies. This convective heat transfer depends on the system's geometry and the experimental conditions. For an isothermal disc, several correlations of the local Nusselt number as a function of the rotational Reynolds number are written as follows:

$$Nu_\infty = Cf(Pr)Re^{*0.5} \tag{1}$$

The function $f(Pr)$ shows the influence of the Prandtl number on the Nusselt number. Values of the $Cf(Pr)$, obtained by many authors, are given in Table 1. Richardson and Sauders [12] propose a correlation including the Prandtl number:

$$Nu_\infty = 0.4Pr^{1/3}Re^{*0.5} \tag{2}$$

The convective heat transfer from an isothermal disc rotating in still air has also been studied by Jackson [13] and

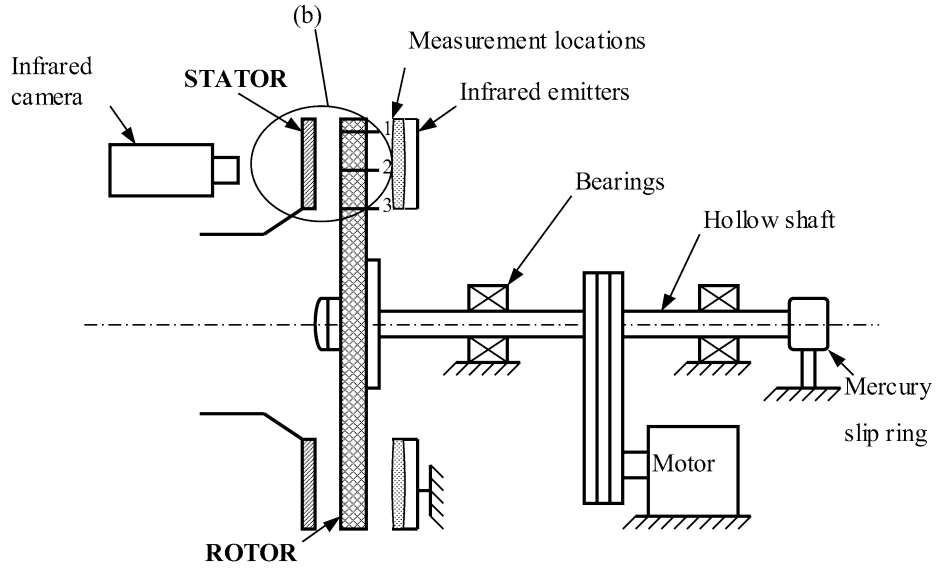

(a)

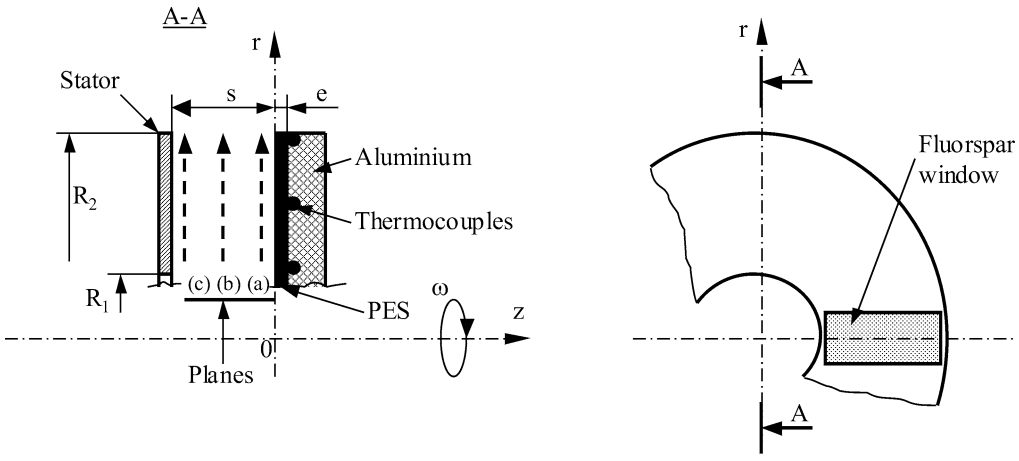

(b)

Fig. 1. Experimental set-up.

Table 1
$Cf(Pr)$ values obtained by different authors

	$Cf(Pr=0.72)$	$Cf(Pr=1)$
Oehlbeck [3]	0.341	0.394
Dorfman [4]	0.322/0.343	0.391/0.399
Sparrow–Gregg [5]		0.396
Wagner [6]	0.335	
Millsaps [7]	0.280	
Hartnett [8]	0.330	
Kreith [9]	0.345	0.380
Popiel [10]	0.330	
Goldstein [11]	0.380	

Cobb [14]. These two authors propose correlations giving the local Nusselt number Nu_∞:

For a laminar flow [13]:

$$Nu_\infty = 0.32 Re^{*0.5} \tag{3}$$

For a turbulent flow [14]:

$$Nu_\infty = 0.019 Re^{*0.8} \tag{4}$$

Dorfman [4] studied the convective heat transfer from a disc rotating in still air and showed the link between the convective heat transfer on the disc and its surface law temperature distribution. In the case of a free disc with a power law temperature profile $T(r) = T_\infty + cr^n$, Dorfman [4] proposes some correlations giving the local Nusselt number Nu_∞:

For a laminar flow ($Re \leqslant 1.82 \times 10^5$), he suggests:

$$Nu_\infty = 0.308 f(Pr) \sqrt{n+2}\, (Re^*)^{0.5} \tag{5}$$

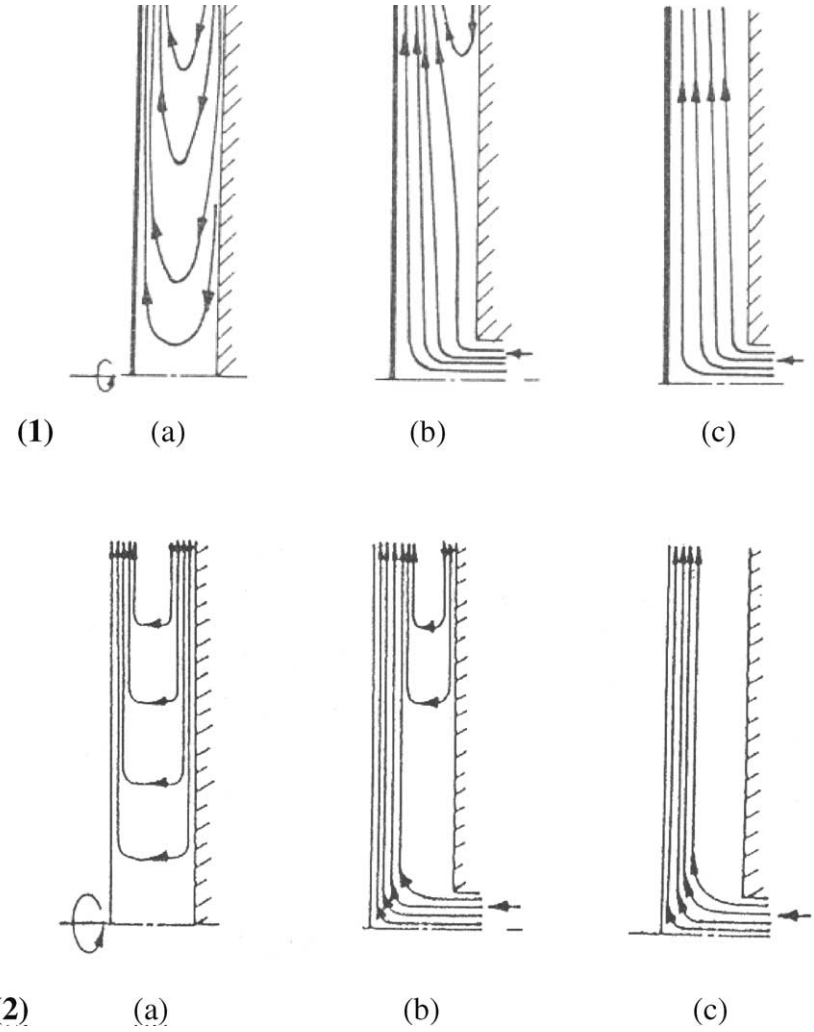

Fig. 2. Flow fields in the air gap, Soo [17], (1) small gap ratio G; (2) large gap ratio G, (a) null airflow; (b) weak air outflow; (c) large air outflow.

where $f(Pr = 0.72) = 0.86$.

For a turbulent flow ($Re \geqslant 2.82 \times 10^5$):

$$Nu_\infty = 0.0197(n + 2.6)^{0.2}(Re^*)^{0.8} \tag{6}$$

The analysis of results described in the literature shows that the suggested correlations depend on the experimental conditions, the system's geometry and the law temperature distributions. It is the same for the *Re* value corresponding to the transition between the laminar and turbulent flows.

In the case of rotor–stator systems, we can classify the geometrical configurations studied in literature into two categories: a rotor facing a stator without a central opening (Figs. 2(1a) and 2(2a)) and a rotor facing a stator with a central opening. The role of the central opening is either to inject an air flow in the gap, or to facilitate free air movement in the space (Figs. 2(1b), 2(1c), 2(2b) and 2(2c)). In our work, the stator has a central opening but no airflow is injected into the gap between the rotor and the stator.

2.1. Stator with a central opening and without an imposed airflow

In this case, many authors [15,16] distinguish four flow regimes depending on the rotational speed and the gap between the rotor and the stator. Regime I, corresponding to laminar boundary layers developed on the two parallel surfaces which touch, is obtained for small gap ratios. Regime II is obtained for a high G value when there are two laminar boundary layers, one on the rotor, another one on the stator, separated by a core of fluid rotating at 0.4ω approximatively. Regime III and IV are respectively equivalent to regime I and II, but for turbulent boundary layers. Owen [15] studied experimentally the mean convective heat transfer in a turbulent flow on a rotating disc facing a stator of the same diameter, with a small central opening and with no airflow imposed in the air-gap. Owen's results [15] are given for a disc with a quadratic temperature profile $T(r) = T_\infty + c \cdot r^2$, parallel to an isothermal stator at T_∞. The author deduced from his results that for low values of G (corresponding to regime III), where $G < 0.01$, a viscous Couette flow region extends from

the rotor to the stator, causing large shear stresses which consequently give rise to Nusselt numbers in excess of the free disc level. As long as $G < 0.01$, the Nusselt number is a decreasing function of G. For the intermediate values of $G(0.01 \leqslant G < 0.06)$. Owen [15] showed that when there are two boundary layers, one on the rotor and another on the stator separated by a rotating core of fluid, the rotating core of fluid reduces shear stress on the rotor and thus the value of the mean Nusselt number falls below that of the free disc. For these values of G, the Nusselt number is an increasing function of G. Furthermore, in his representation of $\overline{Nu}$ as a function of G for fixed Reynolds numbers, Owen [15] showed that there is a gap ratio G $(G = 0.01)$ for which the mean Nusselt number is the minimum, which corresponds to the limit between regime III and regime IV.

When the G value increases again $(G \geqslant 0.06)$, Owen [15] deduces from his results that the core rotation becomes weaker and finally the fluid flow becomes similar to that obtained near a free disc. This causes an increase in the Nusselt number which is close to that of a free disc. His experimental results are asymptotically near to a constant value slightly higher than that obtained in the case of the free disc.

Owen [15] put forward an equation giving the boundary value of G above which the Nusselt number and the flow structure in the gap are not affected by the presence of the stator. This boundary value of G depends on the rotational Reynolds number:

$$G_{\lim} = 1.05Re^{-0.2} \tag{7}$$

2.2. Stator with a central opening and an imposed airflow

Soo [17] studied theoretically the laminar flow structure in a rotor–stator system with an imposed airflow at the centre of the stator. He showed that the flow structure for a small gap between the two discs depends on the parameter $\Phi(x)$:

$$\Phi(x) = \frac{G \cdot C_w}{2\pi Re_s^2} \frac{1}{x^2} \tag{8}$$

where $C_w = Q_m/\mu r$, is the mass flow rate coefficient, $Re_s = \omega s^2/\nu_a$: gap Reynolds number and $x = r/R_2$: dimensionless radius.

Fig. 2(1) shows the typical streamline patterns of the laminar flow for a small air gap and for different values of $\Phi(x)$ [17]. If there is no airflow from the stator $(\Phi(x) = 0)$, the flow structure is of the Couette type with an outflow on the rotor and an inflow on the stator (Fig. 2(1a)). For a small air flow $(\Phi(x) = 1/180)$, the flow structure is outward on the rotor, whereas on the stator periphery there is a separation of the flow with an inflow zone (Fig. 2(1b)). When the fluid flow entering the air-gap increases $(\Phi(x) = 1/90)$, the flow becomes gradually inward in the whole gap (Fig. 2(1c)).

Soo [17] also presents the typical streamline patterns of the laminar flow for large gaps between the rotor and the stator, and for different airflows injected at the stator opening (Fig. 2(2)). The author shows that in this case, the flow structure depends on the parameter X_0:

$$X_0 = \left(\frac{C_w Re^{-1/2}}{\pi}\right)^{1/2} \tag{9}$$

When $X_0 < 1$ (Figs. 2(2a) and (2b)), the flow is of the Batchelor type [18] with a radial outflow on the rotor and a radial inflow on the stator, separated by a core of fluid rotating at approximatively 0.38ω. The radial velocity component is null in this core of fluid. When $X_0 > 1$ (Fig. 2(2c)), the flow is of the Stewartson type [19], with an outflow on the rotor and without a formation of a rotating core of fluid.

2.3. Stator without a central opening

Daily and Nece [16] studied theoretically and experimentally the flow structure in the case of a shrouded rotor–stator system and a stator without central opening. Tests were carried out for rotational Reynolds numbers ranging from 10^3 to 10^7 and for gap ratios $G = 0.0127, 0.0255, 0.0637, 0.115$ and 0.217. Daily and Nece [16] showed that there were also four flow regimes depending on the rotational Reynolds number and the gap ratio. These authors propose some empirical equations giving the moment coefficient for one side of the rotor, valid for a laminar flow:

$$C_m = \pi G^{-1} Re^{-1} \quad \text{(small gap, regime I)} \tag{10}$$

$$C_m = 1.85 G^{1/10} Re^{-1/2} \quad \text{(large gap, regime II)} \tag{11}$$

These results (Eqs. (10) and (11)) were also obtained theoretically by Owen [15], in the case of a shrouded rotor–stator system, a stator without a central opening and a laminar flow. Owen [15] uses the Reynolds analogy to establish correlations expressing the mean Nusselt number on the rotor as a function of the dimensionless parameters Re and C_m $(\overline{Nu} = ReC_m/\pi)$, valid for a Prandtl number equal to 1, a quadratic temperature profile of the rotor surface $T(r) = T_\infty + c \cdot r^2$ and a laminar flow:

$$\overline{Nu} = G^{-1} \quad \text{(small gap, regime I)} \tag{12}$$

$$\overline{Nu} = \frac{1.85}{\pi} G^{1/10} Re^{1/2} \quad \text{(large gap, regime II)} \tag{13}$$

In conclusion, the studies described in literature show the importance of the following on the convective heat transfer from the rotor: the system's geometry, the gap between the two discs, the existence of a central opening in the stator, the flow crossing the air gap, the rotational speed of the rotor and the law of the temperature distribution on the discs surface.

3. Tests description

3.1. Experimental set-up

The experimental study of the local convective transfer is carried out on a rotor facing an isothermal crown stator

(Fig. 1 (a) and (b)). The two discs are spaced from $s = 3$ to 50 mm. The study zone of the convective transfer on the rotor lies between the radii $R_1 = 170$ mm and $R_2 = 290$ mm. In the literature we have not found a study on a similar geometry that is to say with a large central opening of the stator. The most commonly used experimental method to determine local convective exchanges is that of the thermally thin wall which allows one to impose temperature distributions of the studied surface. In practice, the thermally thin wall is a metal foil and its application on rotating surfaces can be delicate. In order to cope with this difficulty, we used an experimental technique based on the use of a thermally thick wall and the numerical resolution of the steady state heat equation to determine the local heat transfer coefficient. In the experimental set-up (Fig. 1), the rotor is made of a highly conductive part (aluminium 43 mm thick and 230 $\mathrm{W{\cdot}m^{-1}{\cdot}K^{-1}}$ thermal conductivity) and a less conductive part modified by additives (Polyethersulfone: PES 2 mm thick and 0.36 $\mathrm{W{\cdot}m^{-1}{\cdot}K^{-1}}$ thermal conductivity). The PES part is stuck on the aluminium disc (Fig. 1(b)) with an epoxy adhesive with a high conductivity. Two peripheral lines of screws surrounding the study zone reinforce the fixing of the two parts. This assembly copes with the problems of contact resistance between the two materials. The high value of aluminium conductivity and the disc thickness homogenize the temperature at the aluminum/PES interface, whereas the low values of PES conductivity and thickness represent experimentally the variations of the local convective exchange. These variations are highlighted by differences in temperature on the rotor surface subjected to cooling. During a test, the rotor is heated by infrared emitters and cooled on the covered face turned towards the clearance by the flow induced by the rotation of the disc. The rotor rotational speed ω varies from 100 to 300 $\mathrm{rev{\cdot}min^{-1}}$. When there is a steady thermal state, the PES surface temperature is determined by infrared camera through a fluorspar window (Fig. 1(b)). The fluorspar transmission coefficient obtained by calibration, is $\tau_f = 0.95 \pm 0.03$ in the camera wavelength rage ($2\ \mu\mathrm{m} < \lambda < 5\ \mu\mathrm{m}$). The temperatures at the PES/aluminum interface are measured by three thermocouples bound to the acquisition system with a mercury ring rotating collector. The precisions on the rotor temperature and the temperature at the PES/aluminum interface are estimated respectively at $\Delta T = \pm 0.9$ K and ± 0.3 K. The air reference temperature T_∞ is measured by a thermocouple in the test room. The absolute error on T_∞ is estimated at $\Delta T_\infty = \pm 0.3$ K. The stator temperature is measured by two K type thermocouples located at two different radii on its surface parallel to the rotor. The absolute error on the stator temperature is estimated at $\Delta T = \pm 0.4$ K. For all the tests, the stator temperature is quasi-uniform and the stator is considered isothermal. The numerical resolution of the energy equation in the PES using the experimental temperature distributions as boundary conditions, gives the local conductive heat flux on the rotor surface subjected to cooling. The difference in calculation between the conductive heat flux and the radiative heat flux gives rise to the convective heat flux and the local heat transfer coefficient on the rotor surface.

3.2. Determination of the local heat transfer coefficient

In the case of the rotor rotating in still air and facing the stator, the local heat transfer coefficient, h, is independent from the angular position because the system is supposed to be axisymetrical. During a test the disc is heated on one face and cooled on the other. When there is a thermal steady state, the energy equation in the PES is written:

$$\frac{\partial^2 T}{\partial r^2} + \frac{1}{r}\frac{\partial T}{\partial r} + \frac{\partial^2 T}{\partial z^2} = 0 \tag{14}$$

The boundary conditions known in the study are (Fig. 1(b)): for $z = 0$, $T_0(r)$ is obtained by infrared thermography, and for $z = e$, $T_e(r)$ is given by the thermocouples. For the boundary conditions on surfaces ($r = R_1; z$) and ($r = R_2; z$), the influence of insulation conditions and a linear temperature variation calculated from the surface temperature measurements have been studied. Thus, it has been deduced that the influence of these two different boundary conditions on the results is limited to very small peripheral zones (near radii R_1 and R_2). Eq. (14) is solved by a finite difference method which gives the temperature field $T(r, z)$. The density of the local conductive heat flux on the rotor's surface subjected to cooling can be calculated by:

$$\varphi_{\mathrm{cd}} = \lambda_{\mathrm{r}}\left(\frac{\partial T}{\partial z}\right)_{z=0} = \varphi_{\mathrm{cv}} + \varphi_{\mathrm{ray}} \tag{15}$$

Where $\varphi_{\mathrm{cv}} = h(T_0(r) - T_\infty)$ represents the convective heat flux from the rotor to the air and $\varphi_{\mathrm{ray}} = \frac{\varepsilon_{\mathrm{r}}}{1-\varepsilon_{\mathrm{r}}}(\sigma T_0^4(r) - J_{\mathrm{r}})$ the radiative heat flux from the rotor towards its environment. Estimation of the rotor's radiosity J_{r} is based on an enclosure constituted of the rotor surface of emissivity $\varepsilon_{\mathrm{r}} = 0.93 \pm 0.02$, the stator surface of emissivity $\varepsilon_{\mathrm{s}} = 0.65 \pm 0.03$, the fluorspar window, the stator central opening and the peripheral crow between the rotor and the stator which behaves like gray surfaces at T_∞. The radiosity is expressed by the following equation:

$$J_i = \varepsilon_i \sigma T_i^4 + (1 - \varepsilon_i)\sum_{j=1}^{5} f_{ij} J_j \tag{16}$$

where ε_i and T_i are respectively the emissivity and the temperature of side (i), and f_{ij}: the form factor of side (i) towards the side (j).

In the range of rotational Reynolds numbers $Re = 5.87 \times 10^4$ to 1.76×10^5, the ratio $\varphi_{\mathrm{ray}}/\varphi_{\mathrm{cv}}$ varies between 42 and 50%. The radiative heat flux from the rotor represents an important part of the whole heat flux and must be taken into consideration when computing h.

The local heat transfer coefficient and local Nusselt number are then deduced:

$$h = \frac{\lambda_{\mathrm{r}}(\frac{\partial T}{\partial Z})_{z=0} - \frac{\varepsilon_{\mathrm{r}}}{1-\varepsilon_{\mathrm{r}}}(\sigma T_0^4(r) - J_{\mathrm{r}})}{T_0(r) - T_\infty} \quad \text{et} \quad Nu = \frac{hr}{\lambda_{\mathrm{a}}} \tag{17}$$

The mean Nusselt number is obtained from the integration of the convective heat flux in the study zone:

$$\overline{Nu} = \frac{\bar{h}R_2}{\lambda_a} = \frac{2R_2}{R_2^2 - R_1^2} \frac{1}{\overline{T_0(r) - T_\infty}} \times \int_{R_1}^{R_2} Nu \cdot \big(T_0(r) - T_\infty\big)\,\mathrm{d}r \quad (18)$$

In these equations T_∞ is the air temperature of the test room. The relative error $\Delta h/h$ on the local heat transfer coefficient is due to the uncertainty of different temperatures and radiative heat flux. The use of uncertainties on each of these variables deduces the total relative error on the local heat transfer coefficient. In the range of rotational Reynolds numbers ($5.87 \times 10^4 \leqslant Re \leqslant 1.76 \times 10^5$) studied where the ratio $\varphi_{ray}/\varphi_{cv}$ is higher, this uncertainty is estimated at 10% [1].

3.3. Mean flow fields

The mean flow fields are obtained by Particle Image Velocimetry (PIV) in different planes between the rotor and the stator. The two discs are spaced similarly to the thermal tests where $s = 3$ to 50 mm. The fluorspar window is replaced by a 5 mm thick glass plate. A water spray, generated by an excited piezoelectric element in the ultrasound band frequency, is added to the flow. The dimensions of the field covered by the objective are 114×110 mm^2. The cross-correlation between two images is carried out on an 850×150 pixels zone. The time interval Δt between images, regulated as a function of the air velocity, ranges between 30 and 400 µs. The mean flow field is calculated with 32 instantaneous fields.

4. Results and analysis

The tests are carried out for rotational speeds ranging from 100 to 300 rev·min^{-1}. Taking into account the values of inner and outer radii of the rotor study zone, this generates a variation of the local Reynolds number Re^* between 2×10^4 and 1.76×10^5.

4.1. Flow structure

The study of the flow field in the air gap between the rotor and the stator is carried out by PIV, for two peripheral Reynolds numbers $Re = 1.17 \times 10^5$ and 1.76×10^5, and for gap ratios G ranging from 0.01 to 0.06. These tests are carried out with an unheated rotor. Only the tests relative to $Re = 1.17 \times 10^5$ are presented here.

The mean flow fields in different planes between the rotor and the stator are obtained in the air gap zone ranging between the radii R_1 and R_2, corresponding to the study zone of the convective exchange. These mean flow fields are presented for three axial positions: near the rotor (a), in the mid-plane between the rotor and the stator (b) and finally near the stator (c) (Fig. 1(b)).

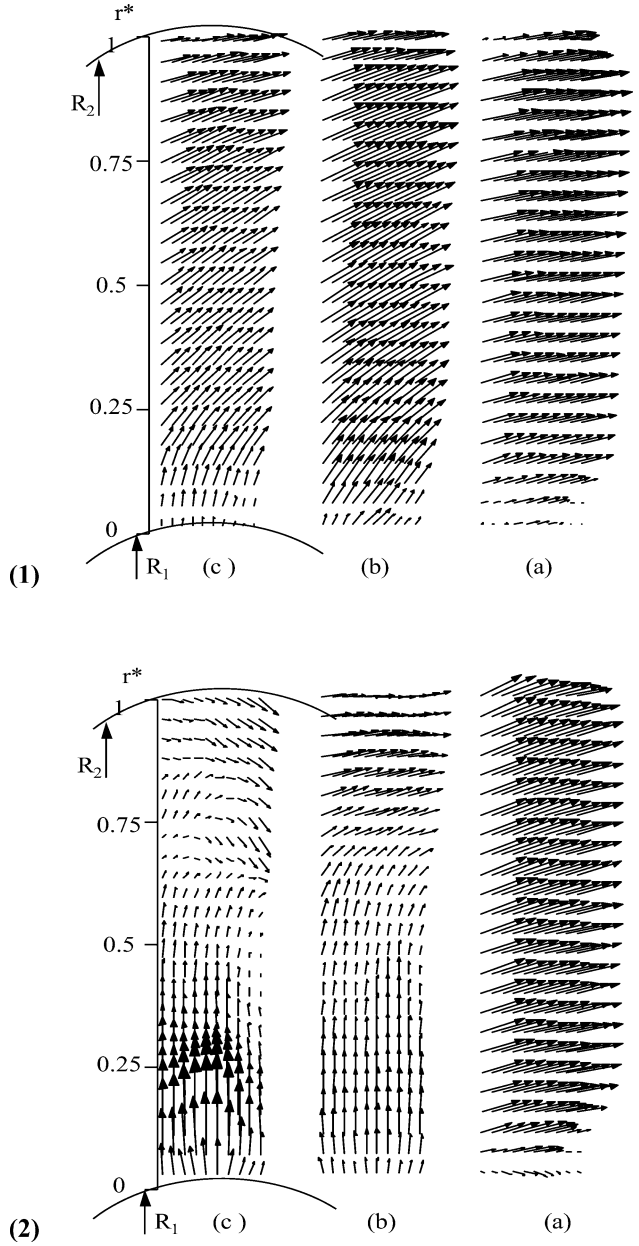

Fig. 3. Flow fields near rotor (a), in the mid-plane between the rotor and the stator (b) and near the stator (c), obtained by PIV $Re = 1.17 \times 10^5$, (1) $G = 0.01$, (2) $G = 0.02$.

For a gap ratio $G = 0.01$, Fig. 3(1) shows that the flow is outward in the whole study zone between the rotor and the stator. The same flow structure was observed for $Re = 1.76 \times 10^5$. The estimation from Eq. (7) of the G_{lim} value at which the flow structure and the convective exchanges on the rotor are not affected by the presence of a stator, shows that in our case ($5.87 \times 10^4 \leqslant Re \leqslant 1.76 \times 10^5$), this G_{lim} value varies between 0.09 and 0.11. For $G = 0.01$, we can expect the stator to have a strong influence on the flow structure, which remains close to the Couette-type flow for

which the viscous region fills the whole space between the rotor and the stator. The section of the stator central opening ($0.09\ m^2$)is much larger than the peripheral section of the air gap ($0.0055\ m^2$),and the fluid aspirated by the rotor flows from the stator opening to the rotor periphery and all the flow is outward in the air gap. Moreover, the measurements of the airflow rate Q_m, induced by the rotation of the rotor, were carried out for gap ratios G ranging from 0.01 to 0.06. The velocity of the air aspirated into the inlet pipe is measured by a Pitot tube connected to a micro manometer and the relative error on the velocity is estimated at ±5%. The aspirated airflow is then determined using the air velocity profile measured in the pipe. For $G = 0.01$, the aspirated mass flow rate varies from 2.6×10^{-3} to 9.1×10^{-3} kg·s^{-1} with the increase in the rotational speed from 100 ($Re = 5.87 \times 10^4$) to 300 rev·min^{-1} ($Re = 1.76 \times 10^5$). In Fig. 4 the parameter $\Phi(x)$ given by Eq. (8) ($\Phi(x) = \frac{G \cdot C_w}{2\pi Re_s^2} \frac{1}{x^2}$), is represented as a function of the dimensionless radius x. In our case, this parameter $\Phi(x)$ depends on the air flow aspirated by the stator central opening. The $\Phi(x)$ boundary values $\Phi(x) = 1/90$ given by Soo [17] are also plotted. The author showed that starting from $\Phi(x) = 1/90$, in other words, for large air flows, the flow remains outward in all the air gap between the rotor and the stator. Fig. 4 shows that the $\Phi(x)$ values obtained in our study for $Re = 1.17 \times 10^5$ and $G = 0.01$ are higher than $1/90$, which explains the presence of an outflow in all the air gap, presented in Fig. 3(1).

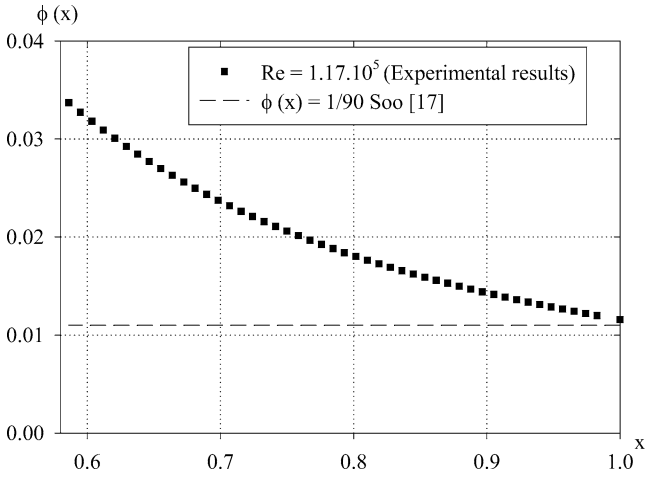

Fig. 4. Ratial evolution of $\Phi(x)$ for $Re = 1.17 \times 10^5$ and $G = 0.01$.

In Figs. 3(2), 5(1) and 5(2) the mean flow fields obtained for gap ratios G ranging from 0.02 to 0.06 are represented for a rotational Reynolds number $Re = 1.17 \times 10^5$. For $G = 0.02$ (Fig. 3(2)), the flow is outward near the rotor (a), where the fluid particles are mainly pushed by the rotation of the rotor. In the mid-plane between the rotor and the stator (b), the flow is radial at the entry ($r^* < 0.6$) then becomes tangential towards the disc periphery ($r^* > 0.6$). Indeed, the thickness of the boundary layers and the interaction of boundary layers built up on the rotor and the stator increase in the flow direction, i.e., towards the disc periphery. This therefore favors a flow in the tangential direction at the high radii. Near the stator periphery (c) ($r^* > 0.6$), an inflow zone can be seen. We find the same characteristics of the flow as those obtained by Soo [17] for a laminar flow and a large gap between a rotor and a stator (Fig. 2(2b)). This author showed that for $X_0 = (\frac{C_w Re^{-1/2}}{\pi})^{1/2} < 1$, the flow structure in the air gap between the rotor and the stator is of

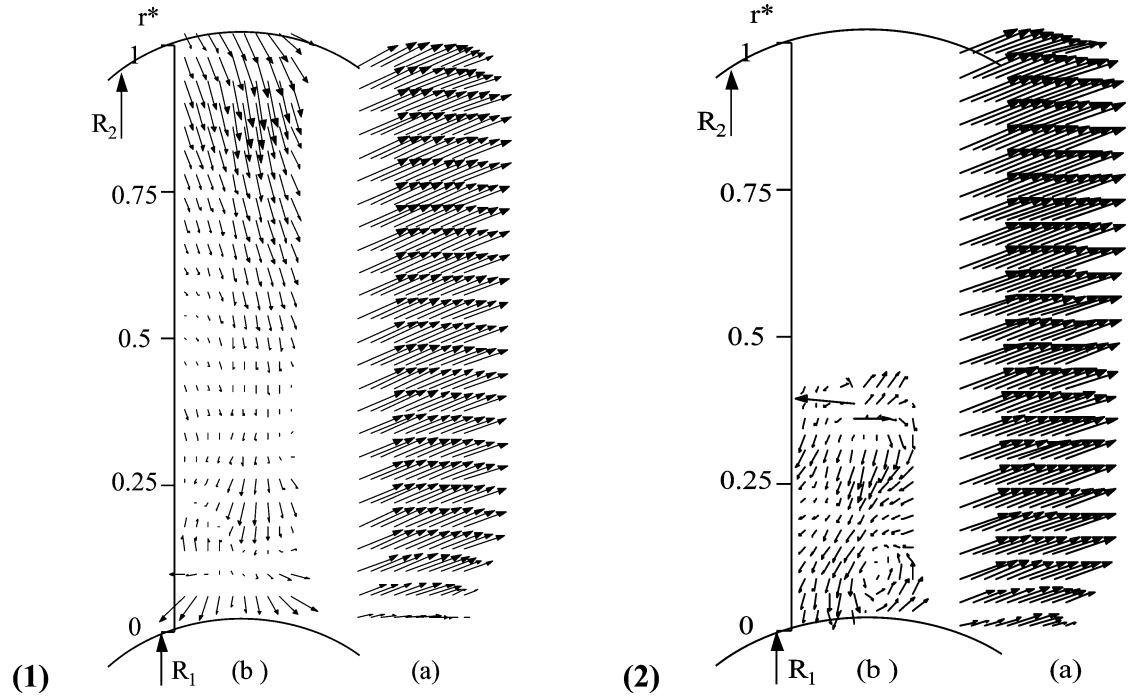

Fig. 5. Flow fields near rotor (a) and in the mid-plane between the rotor and the stator (b), obtained by PIV for $Re = 1.17 \times 10^5$, (1) $G = 0.04$, (2) $G = 0.06$.

the Batchelor type [18]. In our case, X_0 varies from 0.72 to 0.86 for dimensionless radii r^* ranging from 0.6 and 1, and for $Re = 1.17 \times 10^5$ and $Q_m = 3.18 \times 10^{-3}$ kg·s^{-1}, which is in agreement with the presence of an outflow on the rotor and an inflow on the stator. The flow structure observed for $G = 0.02$ seems to be similar to the Batchelor solution [18]. When the G value increases, $G = 0.04$ (Fig. 5(1)), the flow is outward near the rotor (a). In the mid-plane between the rotor and the stator (b), we can distinguish swirling structures at the entry of the air gap ($r^* < 0.25$). Beyond this zone ($r^* > 0.25$), there is a radial inflow. For gap ratio $G = 0.06$ (Fig. 5(2)), the flow is outward near the rotor (a) and in the mid-plane between the rotor and the stator (b), we can distinguish swirling structures at the entry of the air gap for $r^* \leqslant 0.4$. In both Figs. 5 (1) and (2), we notice the absence of fluid particles near the stator. The measurement technique used did not let us obtain the mean flow field near the stator because of the very low velocity values. The flow structure in these two cases is probably similar to the Stewartson type flow [19], where there is only one outward boundary layer on the rotor.

4.2. Velocity profiles

From the mean flow fields (Fig. 6), we illustrate the evolutions of the dimensionless radial and tangential components of air velocity between the rotor ($z'/s = 0$) and the stator ($z'/s = 1$) for the Reynolds number $Re = 1.17 \times 10^5$ and $G = 0.01$. Fig. 6 (a) and (b) show the results for gap ratio $G = 0.01$. For these figures it can be seen that for $0.16 < z'/s < 0.83$, the radial velocity component is z' and r^* decreasing function, and the tangential velocity component is z' decreasing and r^* increasing function. The tangential component values are high near the rotor where the flow is mainly pushed by the rotation. They then decrease when we move away from the rotor in its normal direction z' to become very weak near the stator surface. The flow structure obtained for $G = 0.01$ is close to the Couette-type flow. This flow type, where the viscous effects are significant, is obtained for gap Reynolds numbers ($Re_s = \omega s^2/\nu_a$) lower than 100 [21]. In our case $Re_s = 12.5$ and the velocity profiles obtained confirm Jacques' observations [21].

When the G value increases, the boundary layers on the two discs are separated. Indeed, for $G = 0.02$ and $Re = 1.17 \times 10^5$ (Fig. 6 (c) and (d)), we distinguish two fields: a field near the rotor where the fluid is ejected towards the outside and the flow is outward on all the rotor surface, and a zone on the stator periphery where the flow is inward and the radial velocity component is very weak. When the value of G increases further, only one boundary layer on the rotor is privileged and outside this boundary layer the radial and tangential velocity components are practically null. Thus, for our study, when $G = 0.04$ or 0.06, and $Re = 1.17 \times 10^5$ (Figs. 6(e)–(h)), the values of the radial and tangential velocity are very high near the rotor. These velocity values decrease quickly when we move away in the normal direction of the rotor, to become quasi-null in the median plane between the two discs.

4.3. Experimental temperature profiles

At the PES crown/aluminum disc interface, the variation of the temperatures recorded by the thermocouples does not exceed 0.3 K. Thus, the aluminum disc plays its role correctly by homogenizing the temperature at the PES/aluminum interface between the two materials. Fig. 7 corresponds to the temperature variation $T - T_\infty$ of the surface subjected to cooling, as a function of a radius, for $Re = 1.17 \times 10^5$ and two gap ratios $G = 0.01$ and 0.02. The surface temperature of the rotor is an increasing function of the radius. The temperature variation ($T - T_\infty$) is between 39.5 and 42.5 K, when $G = 0.01$ and between 34 and 35.5 K when $G = 0.02$. The same type of distribution is observed for $G \geqslant 0.04$ as long as the rotating speed remains lower than 300 rev·min^{-1} ($Re = 1.76 \times 10^5$). For all these tests, the reference temperature of the air, T_∞ (air of the test room) is about 293 K. The stator is isothermal at a temperature of about 303 K.

4.4. Local Nusselt number

Fig. 8 shows the radial variation of the local Nusselt number on the rotor for peripheral rotational Reynolds numbers ($5.87 \times 10^4 \leqslant Re \leqslant 1.76 \times 10^5$) and for gap ratios ranging from 0.01 to 0.17. The results relative to the single rotating disc without stator and Dorfman's results [4] on the free disc (Eqs. (5) and (6)) with a power law temperature profile $T = T_\infty + c \cdot r^n$, are also plotted on the same graph. The exponent of this power law is obtained by interpolation of experimental temperature profiles. In our tests the values of n are low: $0.05 \leqslant n \leqslant 0.11$, we are therefore very close to the case of an isothermal disc. In the case of the free disc and $Re = 1.17 \times 10^5$ (Fig. 8(g)) which corresponds to a laminar flow on the single rotating disc [1], the Nusselt number is proportional to the radius, and the local heat transfer coefficient ($h = Nu \cdot \lambda_a/r = cst$) is independent from the radius. The comparison of our experimental results for the free disc with those of Dorfman [4] shows the same tendencies for the evolutions of the local Nusselt number (Fig. 8(g)). The average relative difference between the experimental values of Nu and those of Dorfman [4] is about 49%. This difference can partly be explained by the presence of the heads of the screws on the rotor surface, which are not perfectly leveled and likely to disturb the flow and increase the convective heat transfer on its surface. In the case of the rotor facing the stator and a gap ratio $G = 0.01$ (Fig. 8(a)), the Nusselt number is approximately constant on all the study zone and the relative gap in comparison with an average value is 6%. The local convective exchanges decrease towards the rotor periphery. On the other hand, for values of G ranging from 0.02 to 0.17 (Figs. 8(b)–(f)), the local Nusselt number is an increasing function of the

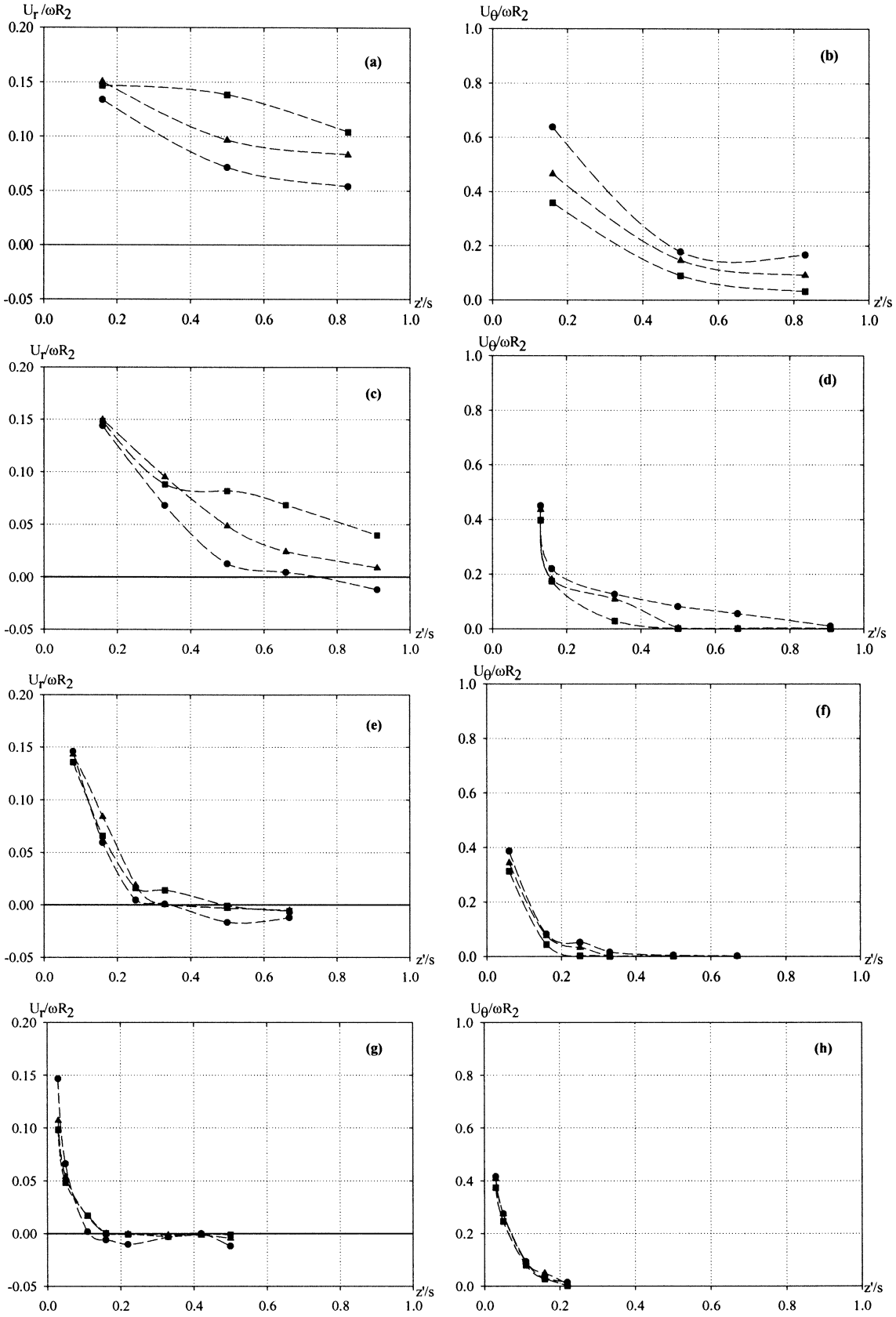

Fig. 6. Evolutions of radial and tangential velocity components measured by PIV, $Re = 1.17 \times 10^5$, $G = 0.01$ (a, b), $G = 0.02$ (c, d), $G = 0.04$ (e, f), $G = 0.06$ (g, h). ■ $r = 0.18$, ▲ $r = 0.22$, ● $r = 0.28$.

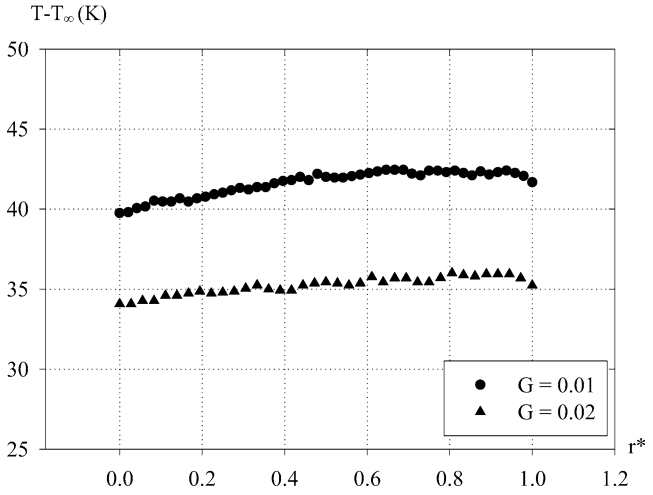

Fig. 7. Temperature profiles on the rotor surface in the study zone ($R_1 < r < R_2$) $Re = 1.17 \times 10^5$.

dimensionless radius r^* and is proportional to r^m. The exponent m remains approximately constant and equal to 1 for all our tests corresponding to $0.02 \leqslant G \leqslant 0.17$. The local heat transfer coefficient ($h = Nu \cdot \lambda_a / r$) is then independent from the radius for this range of G values. For $G = 0.02$, the Nusselt number values are lower than those obtained for $G = 0.01$. These values of the local Nusselt number increase with the increasing function gap ratio G and approach those obtained on the free disc for $G \geqslant 0.04$.

According to our experimental results, the distribution of the local Nusselt number and local heat transfer coefficient as a function of the radius for a gap ratio $G = 0.01$ differs from that obtained for $G = 0.02$ to 0.17. This radial evolution of *Nu* and *h* can also be explained by the thermal boundary layer thickness on the rotor. For $G = 0.01$, the flow structure is closer to the Couette-type flow for which the viscous region fills the whole space between the rotor and the stator [15]. The airflow induced by the rotation of the rotor and imposed by the stator central opening is rejected towards the rotor periphery (Fig. 3(1)). The fresh air supply comes through the stator opening and the fluid in the air gap heats in the flow direction. This corresponds to an increase in the thermal boundary layer thickness because in the air-gap there is no fresh fluid supply to the rotor facing the stator, contrary to the case of the free disc. The air temperature was measured by thermocouples at the air-gap entrance (T_e) and exit (T_p). For the test at $Re = 1.17 \times 10^5$, the measurements are: $T_e = 314$ K and $T_p = 317$ K. These values confirm the fluid heating in the flow direction. The fluid temperature towards the periphery approaches that of the rotor, causing the decrease in the convective heat transfer on the rotor. For $G = 0.02$ and fixed *Re*, the airflow rate induced by the rotation of the rotor decreases and the flow structure is closer to the Batchelor type flow (Fig. 3(2)). The fresh air supply comes through the stator central opening and the discs' periphery. When the G value increases again $G > 0.02$, the airflow rate induced by the rotor and aspired by the stator central opening becomes very low. In this case, the flow structure approaches those obtained on the free disc when the local Nusselt number and the local heat transfer coefficient are proportional to the radius.

Fig. 8(h) illustrates the experimental results for $Re = 1.76 \times 10^5$ ($\omega = 300$ rev·min^{-1}). The results relative to the single rotating disc are now compared to Dorfman's results [4] corresponding to laminar (Eq. (5)) and turbulent (Eq. (6)) flows on the free disc with a power law temperature profile $T = T_\infty + c \cdot r^n$. Although Reynolds numbers on the free disc correspond to the laminar flow (according to Dorfman [4]) our experimental results are closer to Dorfman's results [4] obtained for a turbulent flow. Average relative differences between Dorfman's results (Eqs. (5) and (6)) and our results are 82 and 28%, corresponding to laminar and turbulent flow respectively. In our case, this Reynolds number range probably corresponds to the laminar/turbulent transition. This transition depends primarily on the experimental conditions under which the tests are carried out. In our case, the rotation shaft exceeds the rotor surface on which the local heat transfer coefficient is evaluated. Indeed, if the disc surface is not entirely flat, the laminar flow loses its stability starting from a rotational Reynolds number weaker than that for the flat disc. In the same way, we can obtain the turbulent flow on the disc for Reynolds numbers lower than 2.8×10^5. Particularly, in the case of free disc, Northrop [20] deduced from his experimental study that the flow is turbulent on the disc and that there is no sign of the passage of the laminar to the turbulent flow, even for Reynolds numbers lower than 2×10^5. He attributes this laminar flow instability to an early transition due to the presence of the rotation shaft.

In the case of the rotor facing the stator, the variation of the local Nusselt number and local heat transfer coefficient as a radius function remains similar to that obtained for $Re = 1.17 \times 10^5$ (Figs. 8(a)–(e)).

4.5. Mean Nusselt number

The evolution of the mean Nusselt number given by Eq. (18) as a function of the gap ratio is plotted in Fig. 9, for different peripheral rotational Reynolds numbers. The results relative to the single rotating disc are also plotted.

In the range of Reynolds numbers studied and for $G = 0.01$, the mean Nusselt number on the rotor is higher than Nusselt numbers obtained for various gap ratios G and on the free disc. The flow structure obtained for $G = 0.01$ is of a Couette-type flow (Figs. 3(1), 6(a) and 6(b)) corresponding to large shear stresses in the fluid compared with those obtained on the free disc. This leads therefore to an increase in the Nusselt number compared to that obtained in the case of a single rotating disc. For $G = 0.02$, the mean Nusselt number obtained is minimal. The flow structure obtained in this case (Figs. 3(2), 6(c) and 6(d)) is close to the Batchelor-type flow. The rotating core of fluid reduces shear stress on the rotor and the value of $\overline{Nu}$ therefore falls

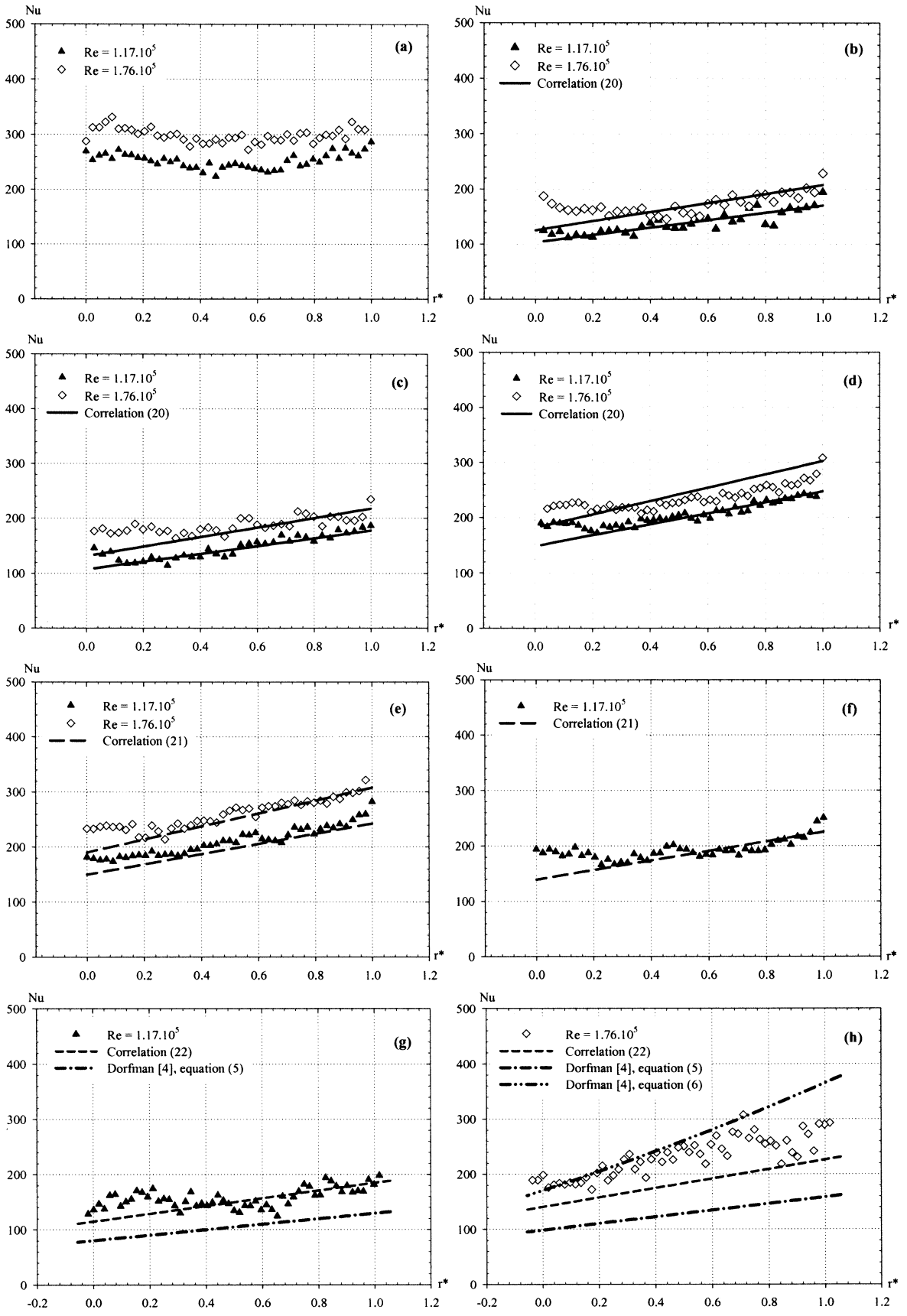

Fig. 8. Local Nusselt number, (a) $G = 0.01$, (b) $G = 0.02$, (c) $G = 0.04$, (d) $G = 0.06$, (e) $G = 0.1$, (f) $G = 0.17$, (g and h) free disc.

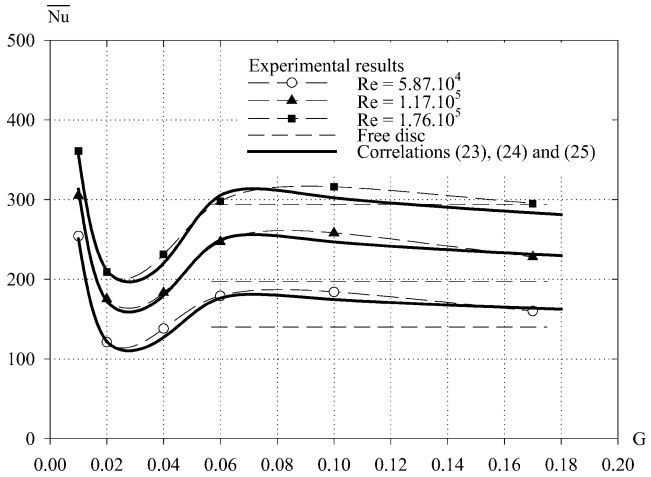

Fig. 9. Mean Nusselt number as a functions of G.

below that of the free disc. For gap ratios higher than 0.02, the mean Nusselt number increases with the increase in the gap between the two discs and is nearer to those obtained on the free disc. The flow structure obtained in this case (Figs. 5(1), 5(2), 6(e)–(h)) is closer to the Stewartson-type flow, where there is only one outward flow on the rotor. Moreover, regardless of the size of the gap between the two discs, the mean Nusselt number increases with the increase in the rotational Reynolds number. This increase of the convective heat transfer on the rotor is due to the reduction in the thickness of the boundary layer. We deduce from our study that for $G < 0.02$ we have an example of a small clearance (regime I), where the mean Nusselt number is a G decreasing function. On the other hand, for $G \geqslant 0.02$, an increase of the gap between the two discs involves an increase in the mean Nusselt on the rotor (regime II). The value of $G = 0.02$, for which the mean Nusselt number is minimal, corresponds to the transition between regime I and II. These results show the agreement between the flow structure and the convective exchange.

In Figs. 10(a) and (b), we compared our experimental results obtained for gap ratios ranging from $G = 0.01$ to 0.17 with the correlations of Owen [15], Daily and Nece [16]. These correlations (Eqs. (12) and (13)) are obtained in laminar flow for the small and large gaps between the two discs corresponding to regime I and II, respectively. For the gap ratio $G = 0.01$ (Fig. 10(a)), our experimental results are higher than those of Owen [15], Daily and Nece [16]. For large gaps $G = 0.02$ (Fig. 10(b)) the results of our tests are slightly higher than those of these authors. The average relative difference in this case is of about 25%. For gap ratios $G = 0.06$, our experimental values of $\overline{Nu}$ are 60% higher than those given by Owen [15], Daily and Nece's correlations [16]. These experimental values of $\overline{Nu}$ decrease with the increase in gap ratio and are near to those obtained on the free disc for $G \geqslant 0.17$. For $G = 0.01$ (regime I), the mean Nusselt number is proportional to $Re^{0.32}$ in our case, whereas it is independent from Re in the case of Owen [15], Daily and Nece [16] (Fig. 10(a)). On the other hand, for

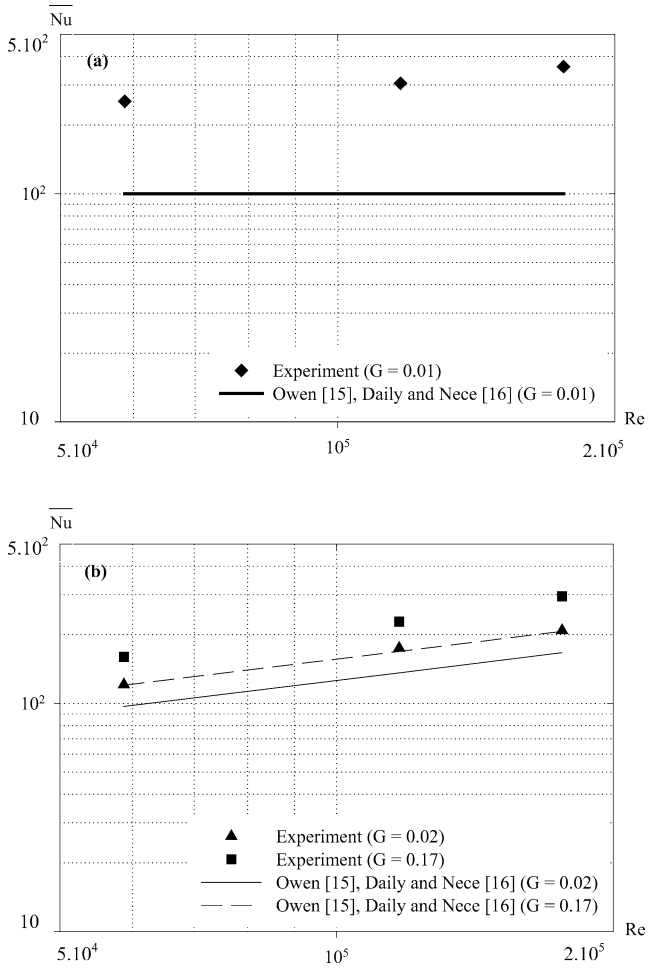

Fig. 10. Comparison of our experimental results with the literature.

$G \geqslant 0.02$ (regime II), the comparison of our experimental results with those of Owen [15], Daily and Nece [16] shows the same tendencies for the evolutions of the mean Nusselt number (Fig. 10(b)). In addition, this comparison also shows that the Nusselt number increases with the gap ratio G for a large gap, whereas it decreases as a function of G for a small gap. The differences observed between our experimental results and those given by these three authors could be justified by the influence of the system's geometry and the thermal limit conditions of different surfaces on the convective exchange. For Owen [15], Daily and Nece [16], the rotor is placed facing a closed stationary plane surface and thus without a central opening. In these authors' studies, the Prandtl number ($Pr = 1$) is different from our $Pr = 0.72$. This difference in the Prandtl number slightly increases the relative difference of the Nusselt numbers corresponding to different gap ratios. The rotor temperature distribution is also different for our tests and those of Owen [15], Daily and Nece [16]. This comparison determines the influence of the aspirated axial airflow and the stator central opening on the convective heat transfer. This airflow is null in the case of Owen [15], Daily and Nece [16] (entirely closed stator) and higher in our case (aspiration air flow by the stator opening).

Generally speaking, the convective exchange increases when the aspirated axial airflow increases. The results of Fig. 10(a) show that the influence of the stator central opening is all the more important since the gap between the two discs is small.

4.6. Correlation of the experimental results

4.6.1. Local convective exchanges on the rotor

The analysis of our experimental results shows that we can correlate all our tests by an equation expressing the local Nusselt number on the rotor as a function of the gap ratio G and of the local rotational Reynolds number Re^*. This equation can be written in the form:

$$Nu = C\,X\,Re^{*m} \tag{19}$$

C and m are constant and X is a function of G.

For $G = 0.01$, the exponent m is almost null ($m = 0$) regardless of what the rotational Reynolds number may be since the local Nusselt number is almost constant in all the study zone. For values of G ranging from 0.02 to ∞ (∞ corresponding to the tests carried out with the free disc), where the local Nusselt number is an increasing function of the radius, the exponent m remains almost constant and equal to 0.5. Thus, for values of G ranging from 0.02 to 0.06, our experimental results are accurately correlated with Eq. (19), by fixing the following C, X and m values:

$0.02 \leqslant G \leqslant 0.06$

$$C = 0.50, \qquad X = 1 + 5.47 \times 10^{-4} \exp(112 \cdot G)$$

and $\quad m = 0.5$

$$Nu = 0.50\big(1 + 5.47 \times 10^{-4} \exp(112 \cdot G)\big) Re^{*0.5} \tag{20}$$

For a gap ratio $G \geqslant 0.06$, the local Nusselt numbers obtained on the rotor decrease with the increase in G and are near to those obtained on the free disc. Our experimental results in this case can be correlated with the following equation:

$G \geqslant 0.06$

$$C = 0.55, \qquad X = 1 + 0.462 \exp\left(\frac{-13 \cdot G}{3}\right)$$

and $\quad m = 0.5$

$$Nu = 0.55\left(1 + 0.462 \exp\left(\frac{-13 \cdot G}{3}\right)\right) Re^{*0.5} \tag{21}$$

In the case of the single disc, the values of the local Nusselt number are correlated with an equation which corresponds to Eq. (21) when G is near to the infinite:

$$Nu = 0.55 Re^{*0.5} \tag{22}$$

Our tests, correlated with Eqs. (20), (21) and (22) are represented on Fig. 8 in the form of $Nu = f(r^*)$ (in these equations we replace Re^* by $\omega r^{*2}/\nu_a$), for $Re = 1.17 \times 10^5$ and 1.76×10^5 and for the different values of G. The relative difference between the experimental values of the local Nusselt number and the calculated values by (20), (21) and (22) is lower than 5%.

It can be noticed however that for $Re = 1.76 \times 10^5$ (Fig. 8(h)), our experimental results on the free disc are higher than the predictions of the correlation (22). This Reynolds number $Re = 1.76 \times 10^5$ could correspond to a laminar/turbulent transition on the free disc in our case [1].

4.6.2. Mean convective exchanges

For Reynolds numbers ($5.87 \times 10^4 < Re < 1.76 \times 10^5$) and a gap ratio $G = 0.01$, the values of mean Nusselt number were correctly correlated with the power law: $\overline{Nu} = A' Re^m$. For this weak gap ratio $G = 0.01$, the exponent m is worth 0.32. For G ranging from 0.02 to ∞, the correlations of the mean Nusselt number were obtained from the integration of the local Nusselt number correlations (Eqs. (20), (21) and (22)) by using Eq. (18).

$G = 0.01$

$$\overline{Nu} = 7.46 Re^{0.32} \tag{23}$$

$0.02 \leqslant G \leqslant 0.06$

$$\overline{Nu} = 0.50\big(1 + 5.47 \times 10^{-4} \exp(112 \cdot G)\big) Re^{0.5} \tag{24}$$

$G \geqslant 0.06$

$$\overline{Nu} = 0.55\left(1 + 0.462 \exp\left(\frac{-13 \cdot G}{3}\right)\right) Re^{0.5} \tag{25}$$

In the case of the free disc, our experimental results are correlated by the following equation:

$$\overline{Nu} = 0.55 Re^{0.5} \tag{26}$$

Our tests, correlated with Eqs. (23)–(25) are shown in Fig. 9 in the form of $\overline{Nu} = f(G)$. In the case of the free disc, average relative differences between Jackson [13] and Dorfman's equations [4] (Eqs. (3) and (5)) and our (correlation (26)) are about 70 and 44%, respectively. Eqs. (23)–(26) coincide with our tests with a relative difference of less than 5%.

5. Conclusion

The experimental study of the local convective exchanges between the air and surface of a rotating disc facing a stator has given rise to the following conclusions:

For a given rotational Reynolds number and a weak gap ratio $G = 0.01$, the flow is outward in all the air gap. The flow structure is of the Couette-type, corresponding to large shear stresses in the fluid compared to those obtained for a free disc. This leads to an increase of the Nusselt number when compared to the case of a large gap.

For $G = 0.02$, the flow is outward on the rotor and inward on the stator with the formation of a core of fluid rotating between the two discs. This causes a reduction of the tangential shear stresses on the rotor and consequently the Nusselt number becomes minimal and weaker than that obtained in the case of the free disc. When the G value increases further the interaction of the boundary layers built

up on the two discs decreases and the flow structure is near to that obtained on the free disc, involving an increase in the tangential shear stresses inside the boundary layer built up on the rotor. This leads to the increase in the Nusselt number on the rotor which is near to that obtained on the free disc.

Our experimental results obtained on the rotor facing the stator with a central opening were compared with those of Owen [15], Daily and Nece [16], for which the stator is without a central opening. This comparison allowed us to deduce that the presence of a stator central opening increases the Nusselt number, whatever G and Re may be. This increase is all the more important since the air gap is weak and the stator opening is large.

In this article we propose some correlations expressing the local and mean Nusselt numbers on the rotor as a function of the rotational Reynolds number Re and of gap ratio G. Our results are valid in the case of a rotor/stator system with a central opening in the stator and without an imposed airflow. This work is still underway for the analysis of the influence of other stator central openings on the convective exchange on the rotor.

References

[1] S. Harmand, F. Monnoyer, B. Watel, B. Desmet, Echanges convectifs locaux sur une couronne d'un disque en rotation, Rev. Gén. Therm. 87 (1998) 885–897.

[2] S. Harmand, F. Monnoyer, B. Watel, B. Desmet, Local convective heat exchanges on a rotating facing a stator, Internat. J. Therm. Sci. 39 (2000) 404–413.

[3] D.L. Oehlbeck, F.F. Erian, Heat Transfer from axisymmetric sources at the surface of a rotating disc, Internat. J. Heat Mass Transfer 22 (1978) 601–610.

[4] L.A. Dorfman, Hydrodynamic Resistance and Heat Loss from Rotating Solids, Oliver and Boyd, Edinburgh and London, 1963, translated by N. Kemmer.

[5] E.M. Sparrow, J.L. Gregg, Heat Transfer from a rotating disc to fluids of any Prandtl number, J. Heat Trans. T. ASME (1959) 249–251.

[6] C. Wagner, Heat transfer from a rotating disc to air, Appl. Phys. (1948) 837–839.

[7] K. Millsaps, K. Pohlhausen, Heat transfer by laminar flow from a rotating plate, J. Aero. Sci. 19 (1952) 120.

[8] I.P. Hartnett, Heat transfer from a nonisothermal disc rotating in still air, J. Appel. Mech. E 81 (1959) 672–673.

[9] F. Kreith, Convection heat transfer in rotating systems, Adv. Heat Transfer 5 (1968) 129–251.

[10] C.O. Popiel, L. Boguslawski, Local heat transfer coefficients on the rotating disc in still air, Internat. J. Heat Mass Transfer 18 (1975) 167–170.

[11] S. Goldtstein, Proc. Cambridge Philos. Soc. 31 (1935) 232.

[12] P.D. Richardson, O.A. Sauders, Studies of flow and heat transfer associated with a rotating disk, J. Mech. Engrg. Sci. 5 (4) (1963) 336–342.

[13] J.D. Jackson, S.A. Al-Khatani, S. He, Investigation of heat transfer from an imposed axial flow of air to a rotating disk, in: Eurotherm Seminar 46, Heat transfer in Single Phase Flows 4, University of Pisa, Italy, May 3–4, 1995, pp. 123–130.

[14] E.C. Cobb, A.O. Sauders, Heat transfer from a rotating disc, Proc. Roy. London Appl. Math. 236 (1956) 341–351.

[15] J.M. Owen, R.H. Rogers, Flow and Heat Transfer in Rotating-Disc Systems, 1, Rotor–Stator Systems, Research Studies Press LTD, 1989.

[16] J.W. Daily, R.E. Nece, Chamber dimension effects one induced flow and frictional resistance of enclosed rotating disks, J. Basic Engrg. 82 (1960) 217–232.

[17] S.L. Soo, Laminar flow over an enclosed rotating disc, Trans. ASME 80 (1958) 287–296.

[18] G.K. Batchelor, Note on a class of solutions of the Navier–Stokes equations representing steady rotationally-symmetric flow, Quart. J. Mech. Appl. Math. 5 (1951) 29–41.

[19] K. Stewartson, On the flow between two rotating coaxial discs, Proc. Cambridge Philos. Soc. 49 (1953) 333–341.

[20] A. Northrop, J.M. Owen, Heat transfer measurements in rotating-disc systems, Part I: The free disc, Internat. J. Heat Fluid Flow 9 (1) (1988).

[21] R. Jacques, Simulations numériques d'écoulements transitionnels et turbulents dans des configurations de type rotor–stator, Doctorat de l'Université de Paris XI, ORSAY, 1997.